Improved 3D integral imaging reconstruction with elemental image pixel rearrangement

doi: https://doi.org/10.1088/2040-8986/aaa391

Improved 3D integral imaging reconstruction with elemental image pixel rearrangement

Kotaro Inoue[1], Min-Chul Lee[2] , Bahram Javidi[3], and Myungjin Cho[1*]

[1] Department of Electrical, Electronic, and Control Engineering, IITC, Hankyong National University, 327 Chungang-ro, Anseong-si, Gyonggi-do 456-749, Republic of Korea

[2] Department of Computer Science and Electronics, Kyushu Institute of Technology, Fukuoka 820-8502, Japan

[3] Electrical and Computer Engineering Department, University of Connecticut, Unit 4157, Storrs, Connecticut 06269, USA

E-mail: mjcho@hknu.ac.kr

Abstract. Computational reconstruction of integral imaging requires much more computational loads than optical reconstruction because of adding and averaging of many elemental images digitally. Thus, to reduce the computational loads, pixels of elemental images rearrangement technique (PERT) has been proposed. It can reconstruct 3D image very fast, but size of the reconstructed 3D image is different from the conventional computational reconstruction due to no consideration of the empty space between pixels on reconstruction plane. Therefore, in this paper, we propose pixels of elemental image rearrangement technique considering the projected empty space (PERTS) to correct the size of the reconstructed 3D images. To verify and support our proposed method, we carry out the preliminary experiments and calculate structural similarity index.

Keywords. Imaging systems, Three-dimensional image acquisition

MSC code. [65D18] Image analysis, [94A08] Image reconstruction

PACS code. [42.30.Wb] Image reconstruction, [42.15.Eq] Optical system design

1. Introduction

Integral imaging, a passive autostereoscopic three-dimensional (3D) imaging technique, provides full color, full parallax, and continuous viewing points. It does not require an active light source such as a laser. It records multiple 2D images with different perspectives through lenslet array or camera array. These images are called elemental images. To reconstruct 3D images, homogeneous lenslet array in display stage is utilized for optical reconstruction and it can obtain the reconstructed 3D images with high speed. However, it may not be applied to some applications because of the poor resolution of the optical system. Therefore, computational integral imaging reconstruction (CIIR) may be used [1].

Various approaches for CIIR have been reported since it does not require complicated optical devices, it can extract 3D depth map, and it can reconstruct 3D images [2-17]. In conventional CIIR, the reconstructed 3D images can be obtained by shifting and averaging the elemental images via different reconstruction depths. It is very simple, but it needs large computational loads because it shifts and averages all elemental images. In addition, due to the averaging effect, the high spatial frequency of the reconstructed 3D images may be degraded so that the visual quality of the reconstructed 3D image decreases. Also, the depth resolution of CIIR depends on the resolution of elemental images because shifting pixels for various reconstruction depths are determined by the number of pixels for each elemental image. Pixels of elemental image rearrangement technique (PERT) has been proposed to enhance the resolution [11].

In PERT, the reconstruction plane is referred to as the projection plane and each pixel of elemental images is back-projected through virtual pinhole array. The reconstructed 3D image can be obtained by sorting these projected pixels from elemental images. Thus, the resolution of the reconstructed 3D image is the same as the resolution of the image sensor. In addition, by sorting pixels for each elemental image instead of using an averaging process, the high spatial frequency of the reconstructed 3D image is not degraded and the reconstructed 3D image can be obtained faster than the conventional CIIR. Therefore, the visual quality of the reconstructed 3D image in PERT may be more enhanced. Since pixel location is determined by the physical distance between the virtual pinhole array and the projection plane instead of the reference pixels in conventional CIIR, the depth resolution depends on the resolution of the image sensor in PERTS. However, because the space between rearranged pixels is not considered and interpolation process is not used in conventional PERT, the size of the reconstructed 3D image is different from the size of the reconstructed 3D image by conventional CIIR. Therefore, in this paper, we propose a PERT with projected empty space (PERTS). In PERTS, one pixel of the elemental images is magnified on the reconstructed plane so that the reconstructed 3D images have the same image size as the original 3D images. To verify our proposed technique, in this paper, we carry out computer simulations and optical experiments.

The paper is organized as follows. We present the principle of PERT in section 2. Then, in section 3, we describe our proposed method (i.e., PERTS). We show the experimental results in section 4. Finally, we conclude with summary in section 5.

2. Methods

2.1. Pixels of elemental images rearrangement technique

Pixels of elemental images rearrangement technique (PERT) obtains the reconstructed 3D images by rearranging pixels of elemental images on the desired reconstruction plane. Figure 1 shows the concept of PERT. For computational simplicity, in this paper, we consider one-dimension only. In PERT, each elemental image is back-projected through virtual pinhole array (focal length is f) on the plane with reconstruction distance D. Thus, magnification ratio M_D can be determined by

$$M_D = \frac{D}{f} \tag{1}$$

The size of the projected pixel on the reconstruction plane $x_p^{(D)}$ can be calculated by the following equation:

$$x_p^{(D)} = \frac{M_D \times c_x}{EI_x} \tag{2}$$

where c_x is the sensor size and EI_x is the number of pixels for elemental images set, respectively. With Eq. (2), the pixel location matrix of the projected elemental images on the reconstructed plane $\mathbf{P}_n^{(D)}$ can be found by

$$\mathbf{P}_n^{(D)} = n \times \frac{x_p^{(D)}}{2} + (i-1) \times p, \quad \text{for } n = 1, 2, \ldots, N_x \tag{3}$$

where i is the index of virtual pinhole, p is the pitch between virtual pinholes and N_x is the number of pixels for each elemental image, respectively. Since $\mathbf{P}_n^{(D)}$ is randomly distributed, it is sorted by bubble sorting algorithm [18]. Thus, using the sorted pixel index matrix $\mathbf{I}_n^{(D)}$, the reconstructed 3D image matrix $\mathbf{R}_n^{(D)}$ at the reconstruction depth D can be obtained by

$$\mathbf{R}_n^{(D)} = \mathbf{EI}\left(\mathbf{I}_n^{(D)}\right) \tag{4}$$

where **EI** is the elemental images set. The feature of PERT is that the number of pixels for the reconstructed 3D image is the same as the one for elemental images set [4]. In conventional CIIR, the number of pixels for the reconstructed 3D image is approximately the same as the one for a single elemental image when the reconstruction depth is large enough. The visual quality of the reconstructed 3D image by PERT is better than the one by conventional CIIR when elemental images with low resolution are used for reconstruction. However, in PERT, the size of the reconstructed 3D image is different from the size of 3D objects because the empty space

between the projected pixels on the reconstruction plane is not considered. Therefore, to obtain the reconstructed 3D image with the same size as the 3D objects, we need to interpolate the projected pixels by considering the empty space between the projected pixels on the reconstruction plane.

2.2. Pixels of elemental images rearrangement technique considering the projected empty space (PERTS)

Figure 2 illustrates the concept of PERT considering the projected empty space (PERTS). In this technique, we assume that the minimum space between the projected pixels is the size of a single pixel. Then, using pixel location matrix of the projected elemental images on the reconstructed plane, the space matrix between the projected pixels can be calculated by

$$\mathbf{S}_n^{(D)} = \begin{cases} \mathbf{P}_n^{(D)} - \mathbf{P}_{n-1}^{(D)}, & 1 < n \le EI_x \\ 0, & \text{otherwise} \end{cases} \tag{5}$$

The minimum space between the projected pixels, $S_{\min}$ is the minimum value of $\mathbf{S}_n^{(D)}$. Thus, the space matrix between the projected pixels with the minimum space can be written by

$$\mathbf{SP}_n^{(D)} = \frac{\mathbf{S}_n^{(D)}}{S_{\min}} \tag{6}$$

In addition, when the size of the minimum space is a single pixel, the pixel size of elemental images on the reconstruction plane can be found by the following

$$x'^{(D)}_p = \frac{x_p^{(D)}}{S_{\min}} \tag{7}$$

Therefore, the total number of pixels for the reconstructed 3D image can be calculated from Eqs. (6) and (7).

$$\tilde{N}_x^{(D)} = x'^{(D)}_p + \sum_{n=1}^{EI_x} \mathbf{SP}_n^{(D)} \tag{8}$$

In PERTS, the reconstructed 3D images can be obtained by magnifying the size of pixels for elemental images with $x'^{(D)}_p$.

$$\tilde{\mathbf{R}}_n^{(D)} = \frac{1}{\mathbf{O}_n} \sum_{k=1}^{EI_x} \sum_{l=1}^{x'^{(D)}_p} \tilde{\mathbf{R}} \left(l + \sum_{m=1}^{k} \mathbf{SP}_m^{(D)} \right) + \mathbf{EI}\left(\mathbf{I}_k^{(D)}\right) \tag{9}$$

The reconstruction process of PERTS is shown in Fig. 3. First of all, let us consider the data set as depicted in Fig. 3(a). $\mathbf{SP}_n^{(D)}$ is the projected pixel space matrix of the elemental images when the minimum space between pixels is the single pixel. Since $\mathbf{S}_n^{(D)}$ and $\mathbf{SP}_n^{(D)}$ can be obtained by subtracting the distance between the projected pixels, the length of matrix should be calibrated. In this paper, we add zeros prior to the matrix for calibration. $\mathbf{I}_n^{(D)}$ is the housing matrix for the sorted elemental images. **EI** is the elemental images and $\mathbf{EI}(\mathbf{I}_n^{(D)})$ is the reconstructed image by PERT and RGB_n is the color vector of each pixel. In Fig. 3(b), using this data set, the

reconstructed image can be obtained. In Eq. (9), Σk is the total summation of the reconstructed image by PERT from $\mathbf{EI}(\mathbf{I}_k^{(D)})$ in sorted sequence. Σl is the pixel resizing process of the elemental images until the projected pixel size is the same as the $x'_p{}^{(D)}$. Finally, $\mathbf{O}_n$ is the overlapping matrix for the computational reconstruction of integral imaging.

In PERTS, the reconstructed 3D images can be obtained while maintaining the size of the real 3D objects. However, the number of pixels for the reconstructed 3D image is very large because the minimum space between pixels of the projected elemental images on the reconstruction plane is set to be a single pixel. In addition, because the single pixel of the elemental images is magnified by the minimum space, the resolution of the reconstructed image with PERTS is not different from the one with PERT. In other words, the high-resolution reconstructed images can be obtained but the actual resolution is the size of elemental images. Also, the processing speed of PERTS is not fast because it needs pixel rearrangement and magnification.

3. Experiment and discussion

Figure 4 and Table 1 show the experimental setup and conditions for computer simulation and optical experiment. In PERT, when the reconstructed 3D image is obtained by using elemental images with largely different perspectives, the visual quality of the reconstructed image is degraded due to the lack of the number of successive pixels. Therefore, pitch between the cameras is 10mm for computer simulation and optical experimentation. The elemental images by computer simulation and optical experiment are shown in Fig. 5. The number of pixels of the elemental image by computer simulation and optical experiment is set to be 960(H)×720(V) and 675(H)×465(V), respectively for verifying our proposed method (i.e., PERTS can improve the visual quality of the reconstructed images using low-resolution elemental images).

Figure 6 shows the reconstructed 3D images using conventional reconstruction method, PERT, and PERTS in simulation experiment. It is noticed that the size of the reconstructed image in PERTS is the same as the one in conventional computational reconstruction. As shown in Figs. 6, the visual quality of the reconstructed image in PERT is worse than PERTS because the perspectives of elemental images are very large in the computer simulation. On the other hand, PERTS improves the visual quality of the reconstructed image even though the elemental images with large perspectives are used. In the optical experimental results as shown in Figs. 7, the character's star sign on the right hand can be recognized well in PERT. The visual quality of the reconstructed image is improved by PERT due to small perspectives of elemental images but the size is different from the objects. However, in Fig. 7(c) and (f), the visual quality of the reconstructed image is improved and the size is the same as the objects. Therefore, it is observed that in PERTS, the visual quality and size of the reconstructed image are enhanced.

Figure 8 shows the Structural Similarity Index (SSIM) via various reconstruction depths by

PERT and PERTS. SSIM can be calculated with the reference image which is reconstructed with high resolution elemental images by CIIR [1]. The number of pixels of high resolution elemental image by computer simulation and optical experiment is 9600(H)×7200(V) and 10110(H)×7020(V). Note that both PERT and PERTS use resized elemental images which is 960(H)×720(V) and 675(H)×465(V) in each experiment.

$$SSIM\left(x,y\right)=\frac{\left(2\mu_x\mu_y+C_1\right)\left(2\sigma_{xy}+C_2\right)}{\left(\mu_x^2+\mu_y^2+C_1\right)\left(\sigma_x^2+\sigma_y^2+C_2\right)} \tag{10}$$

where μ_x, μ_y, σ_x, σ_y and σ_{xy} represent mean, standard deviation and mutual covariance of image. C_1 and C_2 are regularization constants set according to Wang et al. [19].

Figure 8(a) is the simulation result and Figure 8(b) is the optical experimental result. It is remarkable that the SSIM results of PERTS in both computer simulation and optical experiment are improved dramatically since the SSIM shows that the reconstructed image by PERTS is similar as the reconstructed image by CIIR despite using low resolution elemental images. However, the processing speed of PERTS is slower than that of PERT. For example, the reconstruction time in PERT is approximately 150 *ms* but one in PERTS is about 75 *s* where we implemented our algorithm in Matlab (R2016a) using the high performance computer (CPU: intel core i7-3770K, RAM: DDR3-1333 16GB). This problem will be investigated in the future work.

4. Conclusion

In this paper, we have proposed a new reconstruction method for improving the visual quality of the reconstructed 3D images with the same size as the objects. Our proposed method rearranges the projected pixels of elemental images set on the reconstruction plane and calibrates the empty space between the projected pixels. Therefore, it can improve the visual quality of the reconstructed images and obtain the reconstructed images with the same size as the objects. However, the reconstruction speed of our proposed method is slower than the one of PERT because it considers the empty space between the projected pixels for each reconstruction depth. In the future work, we will investigate this slow processing speed by using graphic processing unit (GPU) and parallel processing. We believe that our proposed technique can be applied to various applications such as preview of 3D imaging system, microscopy, defense, and so on.

Acknowledgement

This research was supported by Basic Science Research Program through the National Research Foundation of Korea(NRF) funded by the Ministry of Education(NRF-2017R1D1A1B03030343) and JSPS KAKENHI Grant Number JP17K06463.

References

[1] S.-H. Hong, J.-S. Jang and B. Javidi, Three-dimensional volumetric object reconstruction using computational integral imaging, *Optics Express* **12**, 483 (2004).

[2] A. Stern, and B. Javidi, 3-D computational synthetic aperture integral imaging (COMPSAII), *Optical Society of America* **11**.19, 2446-2451 (2003).

[3] S.-H. Hong and B. Javidi, Improved resolution 3D object reconstruction using computational integral imaging with time multiplexing, *Optics Express* **12**, 4579 (2004).

[4] M. Martínez-Corral, B. Javidi, R. Martínez-Cuenca, and G. Saavedra, Integral imaging with improved depth of field by use of amplitude-modulated microlens arrays. *Applied Optics* **43**(31), 5806-5813 (2004).

[5] S.-W. Min, K.-S. Park, B. Lee, Y. Cho and M. Hahn, Enhanced image mapping algorithm for computer-generated integral imaging system, *Japanese Journal of Applied Physics* **45**.7L (2006).

[6] B. Javidi, P.-D. Rodrigo, and S.-H. Hong, Three-dimensional recognition of occluded objects by using computational integral imaging, *Optics Letters* **31**.8 (2006).

[7] Y.-S. Hwang, S.-H. Hong, and B. Javidi, Free view 3-D visualization of occluded objects by using computational synthetic aperture integral imaging, *Journal of Display Technology* **3**.1, 64 (2007).

[8] M. Cho and B. Javidi, Three-dimensional tracking of occluded objects using integral imaging, *Optics Letters* **33**, 2737 (2008).

[9] D.-H. Shin, B.-G. Lee, and J.-J. Lee, Occlusion removal method of partially occluded 3D object using sub-image block matching in computational integral imaging, *Optics Express* **16**, 16294 (2008).

[10] D.-H. Shin, and E.-S. Kim, Computational integral imaging reconstruction of 3D object using a depth conversion technique, *Journal of the Optical Society of Korea* **12**.3, 131 (2008).

[11] M. Cho and B. Javidi, Computational Reconstruction of Three-Dimensional Integral Imaging by Rearrangement of Elemental Image Pixels, *Journal of Display Technology* **5**, 61 (2009).

[12] J. Jung, M. Cho, D.K. Dey and B. Javidi, Three-dimensional photon counting integral imaging using Bayesian estimation, *Optics Letters* **35**, 1825 (2010).

[13] J.-J. Lee, B.-G. Lee, and H. Yoo, Image quality enhancement of computational integral imaging reconstruction for partially occluded objects using binary weighting mask on occlusion areas, *Applied Optics* **50**, 1889 (2011).

[14] K. Wakunami, M. Yamaguchi, and B. Javidi, High-resolution three-dimensional holographic display using dense ray sampling from integral imaging, *Optical Society of America* **37**.24, 5103-5105 (2012).

[15] Y. Piao, M. Zhang and E.-S. Kim, Effective reconstruction of a partially occluded 3–D target by using a pixel restoration scheme in computational integral-imaging, *Optics and Lasers in*

Engineering **50**, 1602 (2012).

[16] M.-C. Lee, K. Inoue, N. Konishi, and J.-J. Lee, Depth extraction of partially occluded 3D objects using axially distributed stereo image sensing, *Journal of Information and Communication Convergence Engineering* **13**.4, 275-279 (2015).

[17] M. Cho, M. Daneshpanah, I. Moon, and B. Javidi, Three-dimensional optical sensing and visualization using integral imaging, Proceedings of the IEEE **99**.4, 556-575 (2011).

[18] D. Knuth, The Art of Computer Programming, 3rd ed. Reading, MA: Addison-Wesley, vol. **3**, Sorting and Searching, (1997).

[19] Z. Wang, A. C. Bovik, H. R. Sheikh, and E. P. Simoncelli, Image Quality Assessment: From Error Visibility to Structural Similarity, *IEEE Transactions on Image Processing* **13**.4, 600-612 (2004).

Figures

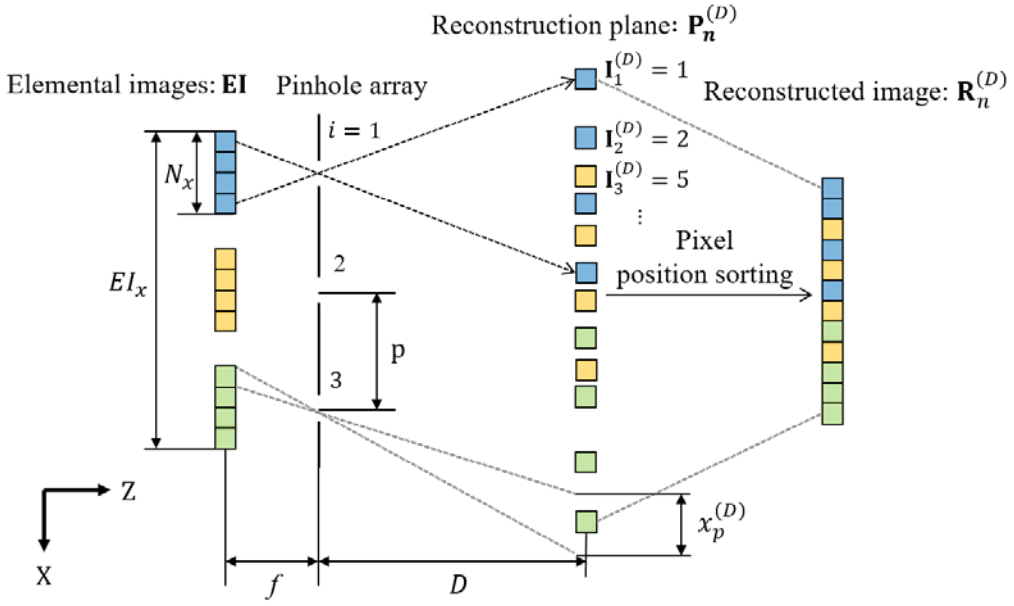

Figure 1. Pixels of elemental images rearrangement technique (PERT)

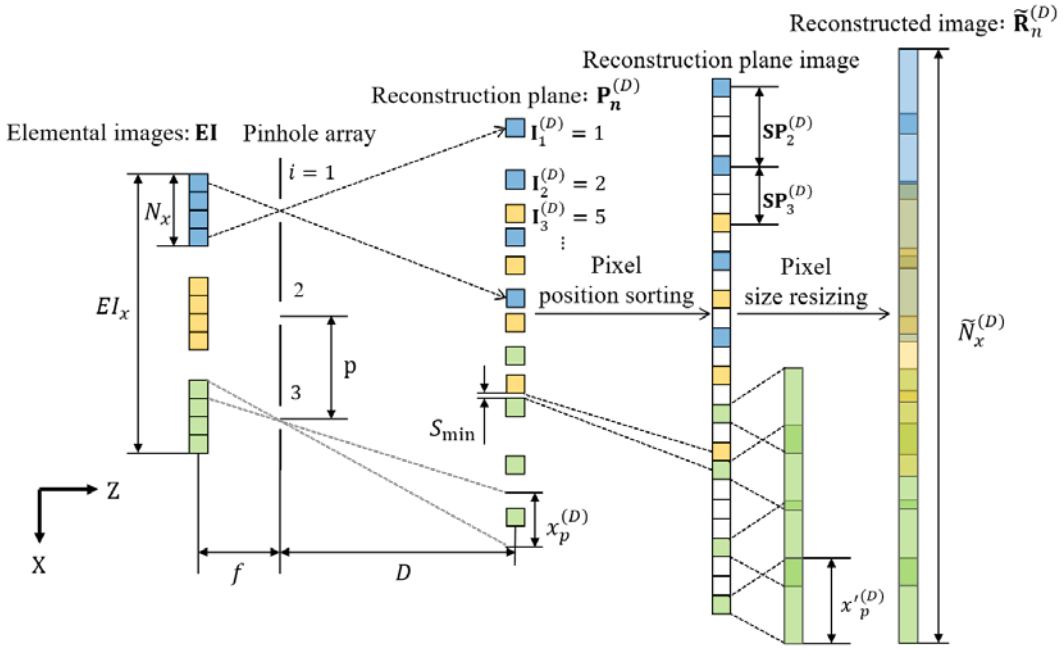

Figure 2. PERT considering the projected empty space (PERTS)

Figure 3. Detail of equations. (a) Data set. (b) Reconstructed image.

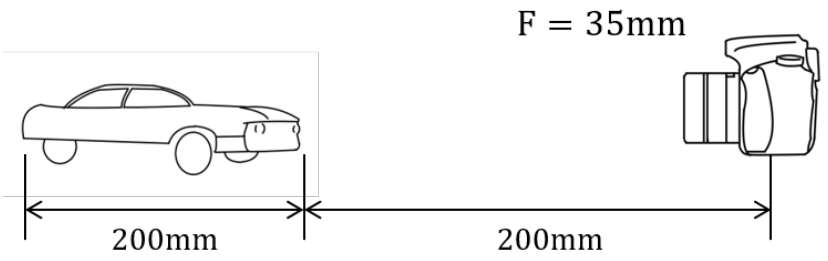

(a)

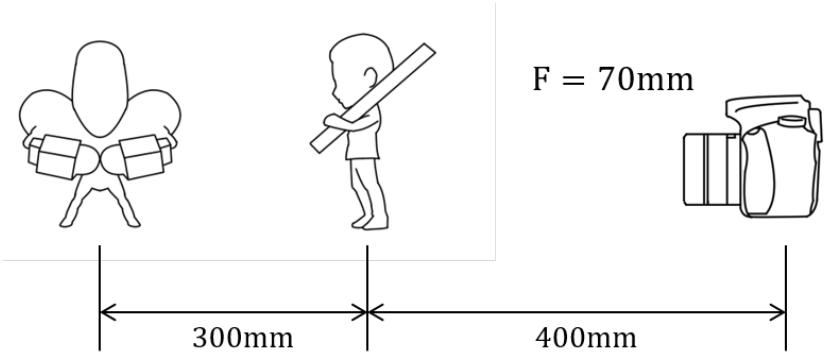

(b)

Figure 4. Experiment setup. (a) Simulation. (b) Optical experiment.

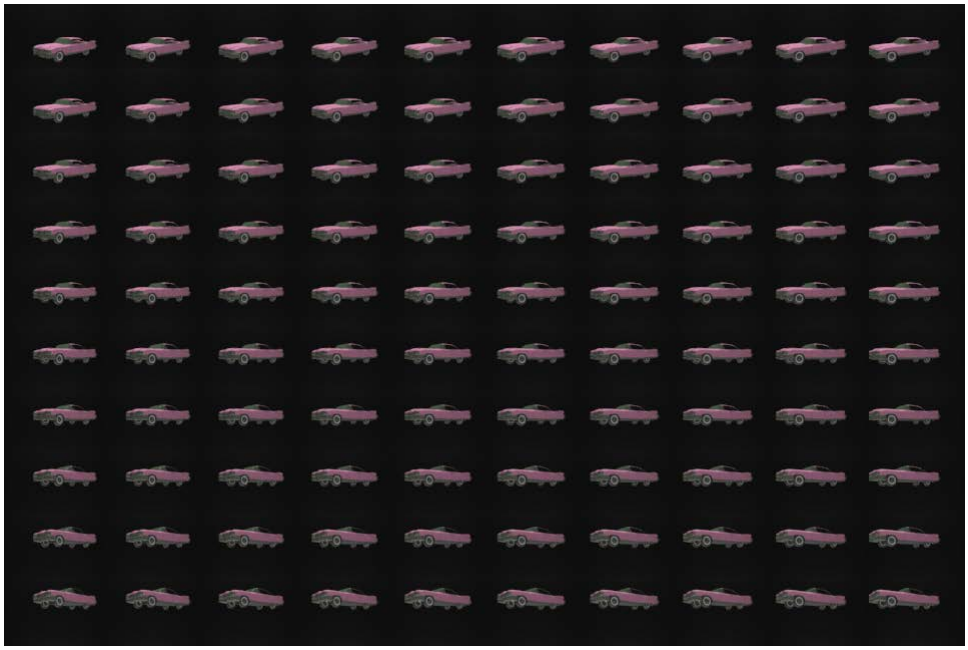

(a)

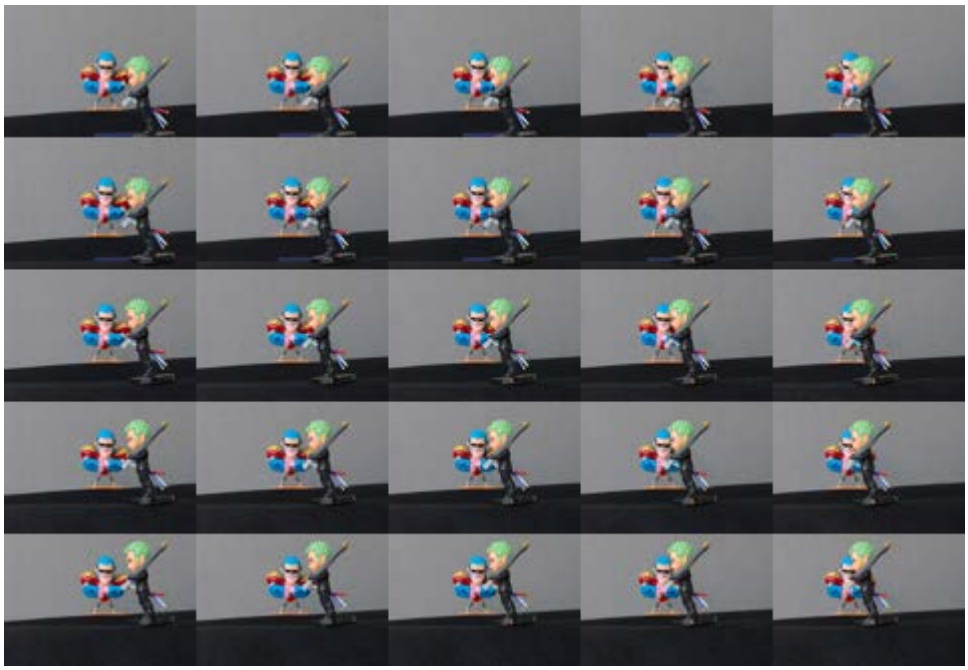

(b)

Figure 5. Elemental images. (a) Simulation. (b) Optical experiment.

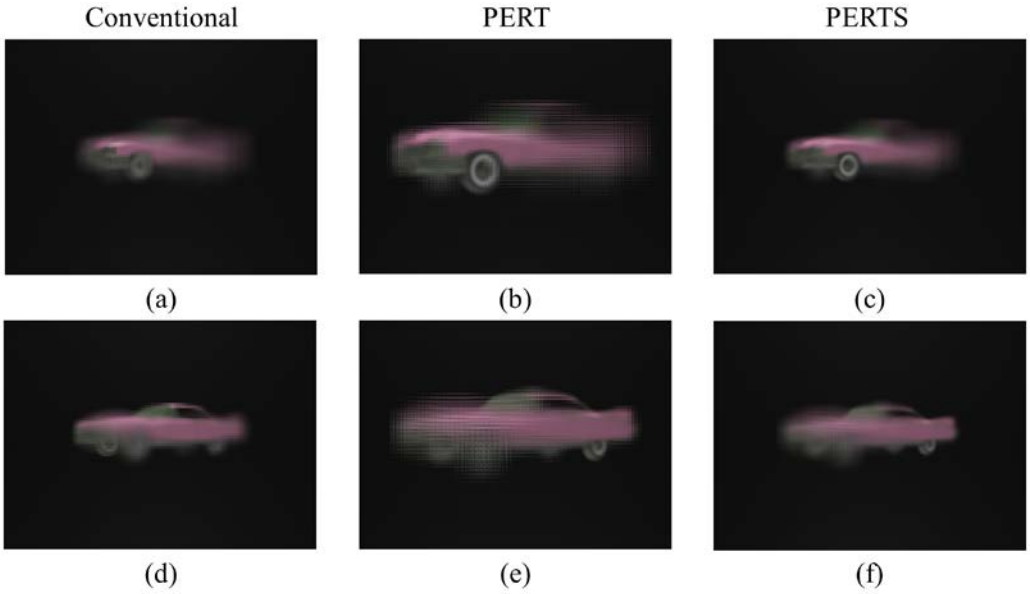

Figure 6. Simulation experimental results, (a)-(c) Reconstruction depth is 250mm. (d)-(f) Reconstruction depth is 350mm.

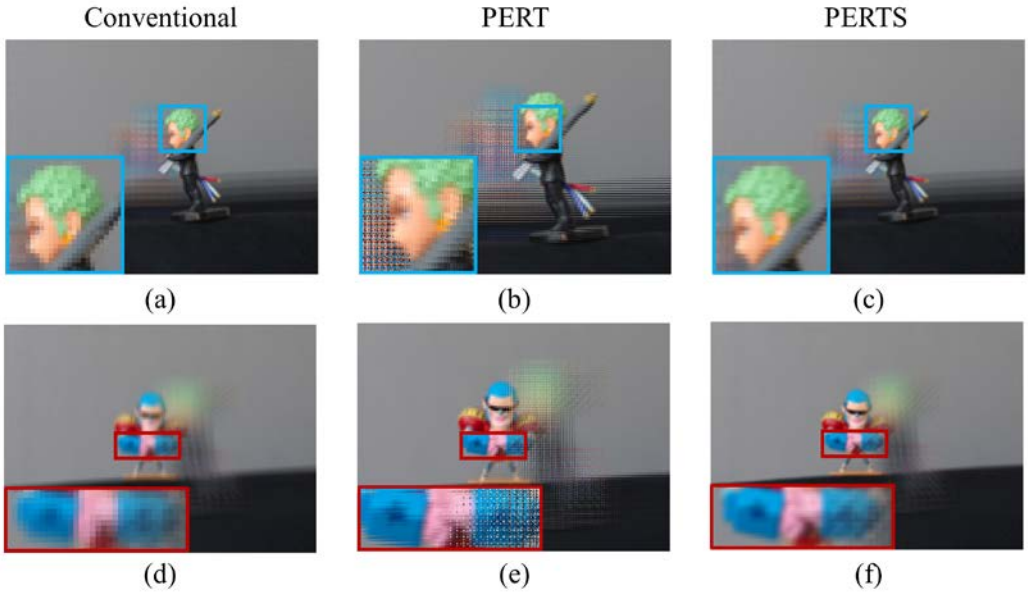

Figure 7. Optical experimental results and its enlarged images, (a)-(c) Reconstruction depth is 340mm. (d)-(f) Reconstruction depth is 600mm.

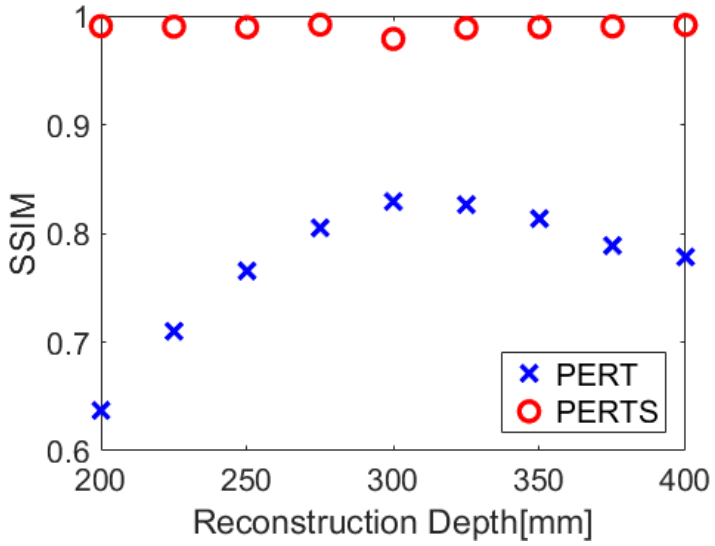

(a)

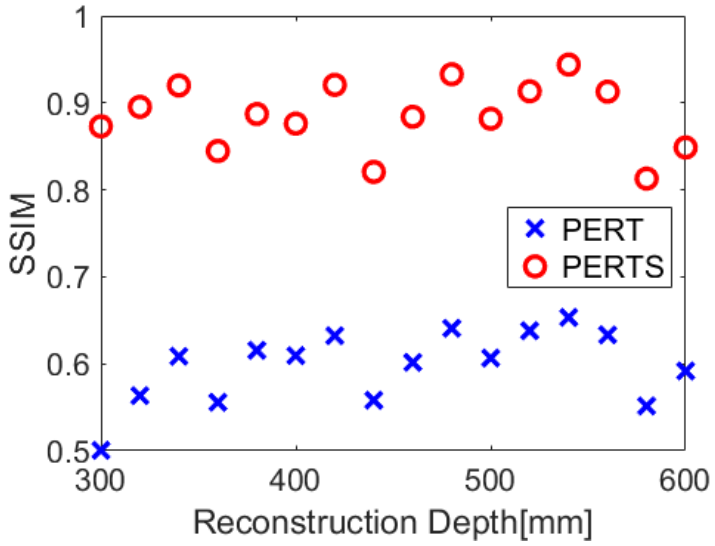

(b)

Figure 8. SSIM via various reconstruction depths. (a) Simulation. (b)Optical experiment.

Tables

Table 1. Experiment setup

	Simulation	Optical experiment
Focal length of the camera	35mm	70mm
Image sensor size	36×24mm	36×24mm
Resolution of each original elemental image	960×720px	2022×1404px
Resolution of each resized elemental image	96×72px	135×93px
Pitch of camera array	10mm	10mm
Number of elemental images	10×10	5×5
Reconstruction depth	200 to 400mm	300 to 600mm
Pitch of reconstruction depth	25mm	20mm